

CMB Faraday rotation as seen through the Milky Way

Soma De¹, Levon Pogosian^{2,3}, Tanmay Vachaspati⁴

¹*School of Earth and Space Exploration, Arizona State University, Tempe, AZ 85287, USA*

²*Department of Physics, Simon Fraser University, Burnaby, BC, V5A 1S6, Canada*

³*Centre for Theoretical Cosmology, DAMTP, University of Cambridge, CB3 0WA, UK*

⁴*Physics Department, Arizona State University, Tempe, AZ 85287, USA*

Faraday Rotation (FR) of CMB polarization, as measured through mode-coupling correlations of E and B modes, can be a promising probe of a stochastic primordial magnetic field (PMF). While the existence of a PMF is still hypothetical, there will certainly be a contribution to CMB FR from the magnetic field of the Milky Way. We use existing estimates of the Milky Way rotation measure (RM) to forecast its detectability with upcoming and future CMB experiments. We find that the galactic RM will not be seen in polarization measurements by Planck, but that it will need to be accounted for by CMB experiments capable of detecting the weak lensing contribution to the B-mode. We then discuss prospects for constraining the PMF in the presence of FR due to the galaxy under various assumptions that include partial de-lensing and partial subtraction of the galactic FR. We find that a realistic future sub-orbital experiment, covering a patch of the sky near the galactic poles, can detect a scale-invariant PMF of 0.1 nano-Gauss at better than 95% confidence level, while a dedicated space-based experiment can detect even smaller fields.

I. INTRODUCTION

The discovery of a primordial magnetic field¹ (PMF) would have a profound impact on our understanding of the early universe [1] and would help explain the origin of the observed magnetic fields in galaxies and clusters [2]. Several observational probes are currently being investigated and the cosmic microwave background (CMB) is a promising tool to discover and study the PMF on the largest cosmic scales.

A PMF can affect the thermal distribution and the polarization of the CMB. The most relevant CMB signature depends on the form of the magnetic field spectrum and also on the level of instrumental noise for different observations. For instance, current CMB bounds of a few nG [3–5] on a scale-invariant PMF [6, 7] derive from temperature anisotropies sourced by the magnetic stress-energy. Comparable bounds were recently obtained in [8] using the Lyman- α forest spectra [9]. As the stress-energy is quadratic in the magnetic field strength, improving this bound by a factor of 2 would require a 16 fold improvement in the accuracy of the spectra. On the other hand, Faraday Rotation (FR) of CMB polarization, being linear in the magnetic field strength, offers an alternative way to improve CMB bounds on a scale-invariant PMF by an order of magnitude [11], and possibly more, with the next generation CMB experiments. Even current CMB data is close to providing competitive bounds on scale-invariant PMF through their FR signature [8, 10].

In contrast, a PMF produced causally in an aftermath of the electroweak or QCD phase transition [12] would have a blue spectrum [13, 14] with most of the power concentrated near a small cutoff scale set by the plasma

conductivity at recombination. It has been suggested [15] that such small-scale fields can appreciably alter the recombination history via enhancement of small scale baryonic inhomogeneities. Consequently, the strongest CMB constraint would come from an overall shift in the distance to last scattering. According to [15], upcoming CMB experiments can rule out causally produced fields with a comoving strength larger than 10^{-11} G.

Given the promise of FR to significantly improve the bounds on scale-invariant PMF [11], it is important to assess the strength of the rotation induced by the magnetic fields in our own galaxy. A rotation measure (RM) map of the Milky Way has recently been assembled by Oppermann et al [16] based on an extensive catalog of FR of compact extragalactic polarized radio sources. They also presented the angular power spectrum of RM and find that it is very close to a scale-invariant spectrum at $\ell \lesssim 200$. Fig. 1 of [16] shows that the root-mean-square RM away from the galactic plane is about 20-30 rad/m². Additional insight into galactic RM on smaller scales can be gained from Haverkorn et al [17] who studied Stokes parameters generated by diffuse polarized sources residing inside the Milky Way. Their power spectra generally agree with the scale-invariance of the large scale tail of the power spectrum of [16], but also show evidence of a break in the spectrum, indicating a power law suppression of the RM power on small scales. Such a break in the RM spectrum is also present in the model of Minter and Spangler [18] who, by fitting to a small set of RM data from extragalactic sources, argued that the spectrum should be set by Kolmogorov turbulence on small scales.

The approximately scale-invariant shape of the galactic RM spectrum can obscure FR constraints on scale-invariant PMF. Based on calculations in [11, 19], one can estimate that a typical galactic RM of 30 rad/m² corresponds to an *effective*, or “energy equivalent” (see Eq. (10) for the definition) PMF strength of 0.6 nG. This

¹ In the context of this paper, “primordial” means that the magnetic field was generated prior to last scattering.

is well below the bounds from Planck [3] obtained using non-FR diagnostics and, as we confirm in this paper, below the levels detectable by Planck via the mode-coupling statistics induced by FR. However, as shown in [11], future CMB experiments capable of detecting the weak lensing B-mode will be able to constrain a scale-invariant PMF of 0.1 nG strength at 100 GHz. Operating at lower frequencies and combining FR information from several channels may further improve the constraints. Clearly, with such high sensitivities the contribution of the galactic RM to the total FR signal will become important.

In this paper, we investigate the imprint of the galactic RM on CMB observables, and its impact on detectability of the PMF via the EB and TB mode-coupling correlations. We start by introducing the necessary concepts and reviewing the known galactic RM measurements in Sec. II. In Sec. III, we estimate detectability of the galactic RM by upcoming and future CMB experiments and forecast future bounds on the scale-invariant PMF under various assumptions. We conclude with a summary in Sec. IV.

II. FARADAY ROTATION OF CMB POLARIZATION

A. Basics of Faraday Rotation

A CMB experiment measures Stokes parameters in different directions on the sky, with parameters Q and U quantifying linear polarization. If CMB photons pass through ionized regions permeated by magnetic fields, the direction of linear polarization is rotated by an angle [20, 21]

$$\alpha(\hat{\mathbf{n}}) = \lambda_0^2 RM(\hat{\mathbf{n}}) = \frac{3}{16\pi^2 e} \lambda_0^2 \int \hat{\tau} \mathbf{B} \cdot d\mathbf{l}, \quad (1)$$

where $\hat{\mathbf{n}}$ is the direction along the line of sight, $\hat{\tau}$ is the differential optical depth, λ_0 is the observed wavelength of the radiation, \mathbf{B} is the “comoving” magnetic field strength (the physical field strength scales with the expansion as $\mathbf{B}^{\text{phys}} = \mathbf{B}/a^2$) and $d\mathbf{l}$ is the comoving length element along the photon trajectory. The rotation measure, RM , is a frequency independent quantity used to describe the strength of FR. Under the rotation of the polarization vector, the two Stokes parameters transform as

$$Q(\nu) + iU(\nu) = (Q^{(0)} + iU^{(0)}) \exp(2i\alpha(\nu)), \quad (2)$$

where $Q^{(0)}$ and $U^{(0)}$ are the Stokes parameters at last scattering. As an approximation, $Q^{(0)}$ and $U^{(0)}$ can be taken to be the observed Stokes parameters at a very high frequency since the FR falls off as $1/\nu^2$.

A PMF contributes to FR primarily at the time of last scattering, just after the polarization was generated, while the mean ionized fraction was still high, and the field strength was strongest. Subsequently, additional FR

is produced in ionized regions along the line of sight that contain magnetic fields, such as clusters of galaxies and our own galaxy. Eq. (1) implies that a significant FR angle can be produced by a small magnetic field over a very large distance, which is the case at recombination, or by a larger magnetic field over a smaller path, which is the case for the Milky Way. We will not discuss FR from clusters which are likely to have a white noise spectrum and contribute to CMB polarization on small scales. We are more concerned with the contribution from the Milky Way that can look very similar to that of a scale-invariant PMF.

In theory, it is possible to extract a map of the FR angle by taking maps of Q and U at different frequencies and using Eq. (2) to solve for the rotation in each pixel. Each additional frequency channel provides a separate measurement of $\alpha(\nu)$ thus reducing the error bar on the measurement of $RM(\hat{\mathbf{n}})$. Such a direct measurement of FR may be challenging when the Q and U signal in each pixel is dominated by noise.

Another way to extract the rotation field is from correlations between E and B modes induced by FR using quadratic estimators [22–26], which is analogous to the method introduced in [27] for isolating the weak lensing contribution to CMB anisotropy. Unlike a direct extraction of FR from Eq. (2), the quadratic estimator method does not utilize frequency dependence and is statistical in nature. It formally involves summing over all pixels of Q and U in order to reconstruct α in a given direction on the sky.

For small rotation angles, the relation between the spherical expansion coefficients of the E, B and α fields can be written as [24]

$$B_{lm} = 2 \sum_{LM} \sum_{l'm'} \alpha_{LM} E_{l'm'} \xi_{lm'l'm'}^{LM} H_{ll'}^L, \quad (3)$$

where $\xi_{lm'l'm'}^{LM}$ and $H_{ll'}^L$ are defined in terms of Wigner 3- j symbols as [24]

$$\xi_{lm'l'm'}^{LM} \equiv (-1)^m \sqrt{\frac{(2l+1)(2L+1)(2l'+1)}{4\pi}} \times \begin{pmatrix} l & L & l' \\ -m & M & m' \end{pmatrix} \quad (4)$$

$$H_{ll'}^L \equiv \begin{pmatrix} l & L & l' \\ 2 & 0 & -2 \end{pmatrix}, \quad (5)$$

and the summation is restricted to even $L+l'+l$. Eq. (3) implies correlations between multipoles of E and B modes that are caused by the FR. Since the primordial T and E are correlated, FR also correlates T and B.

The quadratic estimator method is based on the assumption of statistical isotropy of primordial perturbations. This implies statistical independence of primordial E_{lm} and B_{lm} for different lm pairs, *e. g.* $\langle E_{lm}^* E_{l'm'} \rangle = \delta_{ll'} \delta_{mm'} C_l^{EE}$ for the primordial E-mode. Furthermore, if primordial fields are Gaussian, all of their correlation functions can be expressed in terms of the power spectra. FR introduces correlations between unequal lm and

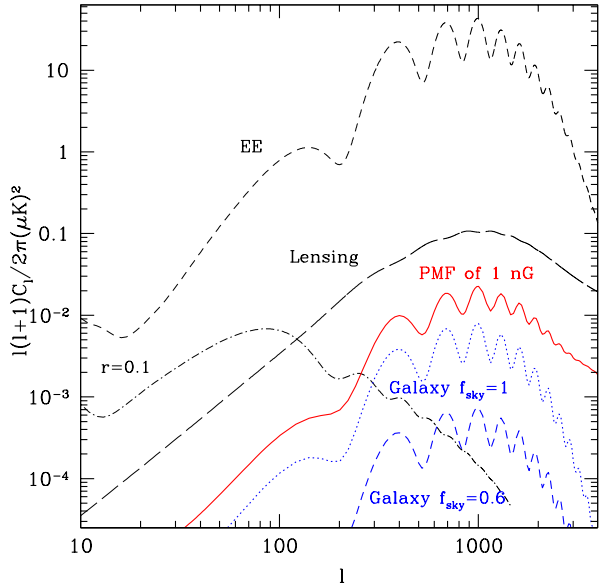


FIG. 1: The CMB B-mode spectrum from Faraday rotation sourced at 30 GHz by a scale-invariant primordial magnetic field of 1 nG strength (red solid), by the full sky galactic magnetic field (blue dot), and by the galactic field with Planck’s sky mask ($f_{\text{sky}} = 0.6$). The black short-dash line is the input E-mode spectrum, the black dash-dot line is the contribution from inflationary gravitational waves with $r = 0.1$, while the black long-dash line is the expected contribution from gravitational lensing by large scale structure.

generates connected four-point correlations. The corresponding non-Gaussian signal can be used to extract the rotation angle. Namely, given a CMB polarization map, one constructs quantities such as [22, 24]

$$\hat{D}_{ll'}^{LM, \text{map}} = \frac{4\pi}{(2l+1)(2l'+1)} \sum_{mm'} B_{lm}^{\text{map}} E_{l'm'}^{\text{map}*} \xi_{lm'l'm'}^{LM} \quad (6)$$

which is the minimum variance unbiased estimator for $D_{ll'}^{LM} = 2\alpha_{LM} C_l^{EE} H_{ll'}^L$ as shown in [28]. Then, each pair of l and l' provides an estimate of α_{LM} via

$$[\hat{\alpha}_{LM}]_{ll'} = \frac{\hat{D}_{ll'}^{LM, \text{map}}}{2C_l^{EE} H_{ll'}^L}. \quad (7)$$

The minimum variance estimator $\hat{\alpha}_{LM}$ is obtained from an appropriately weighted sum over estimators for each ll' pair. If all such pairs were statistically independent, the weighting would be given by the inverse variance of each estimator. However, one has to account for the correlation between the ll' and $l'l$ pairs and a detailed derivation of the appropriate weighting can be found in [22]. Quantities such as $\hat{D}_{ll'}^{LM, \text{map}}$ can also be constructed from products of T and B or, more generally, all possible quadratic combinations, *i.e.* {EB, BE, TB, BT, TE, ET, EE}. One can construct an estimator $\hat{\alpha}_{LM}$ that utilizes all these combinations while accounting for the covariance between them [24]. In this paper, we opt to consider

EB/BE and TB/BT separately, since one of them is typically much more informative than other combinations. For further details of the method the reader is referred to [22, 24].

We will assume a “stochastic” primordial magnetic field such that its value at any given location is described by a probability distribution function. This implies that one can only predict statistical properties of FR, such as the rotation power spectrum, $C_L^{\alpha\alpha}$. The estimator for the power spectrum directly follows from the estimator of α_{LM} and derives from four-point correlations, such as EBEB. In the next section, we will examine detectability of the rotation spectrum caused by the galactic and primordial magnetic fields.

We note that the form of the quadratic estimator allows for contributions from the monopole ($L = 0$) and dipole ($L = 1$) of the FR field which, in principle, should not be ignored. However, the monopole is generally not expected for FR, since it would imply a non-zero magnetic charge enclosed by the CMB surface, while the dipole, corresponding to a uniform magnetic field, is strongly constrained for the PMF and is relatively unimportant for the galactic RM.

In addition to mode-coupling correlations of EB and TB type, FR also contributes to the B-mode polarization spectrum, C_l^{BB} . In Fig. 1 we show the B-mode spectrum at 30 GHz due to FR by a PMF with a scale-invariant spectrum and effective field strength of 1 nG. The B-mode spectrum due to FR by the galactic field is also shown for two choices of sky cuts. For reference, we show the E mode auto-correlation spectrum which acts as a source for the FR B modes, the B modes from inflationary gravitational waves with $r = 0.1$, and the expected contribution from weak lensing (WL). As can be seen from Fig. 1, the shape of the FR induced B mode spectrum largely mimics that of the E-mode, and the galactic contribution has a very similar shape to that of the scale-invariant PMF. A more detailed discussion of the FR induced B-mode spectrum can be found in [19]. As shown in Sec. III, the FR signatures of the galactic or scale-invariant PMF are always less visible in the B-mode spectrum compared to the EB quadratic estimator, with the latter promising to provide the tightest constraints. We note that for causally generated PMF, which have blue spectra with most of the power concentrated at the dissipation scale, the signal-to-noise ratio (SNR) for detecting FR in BB is higher than that in the quadratic estimators [11], although the resulting constraints are not competitive with other probes of causal fields. In what follows, we will focus on FR signatures of scale-invariant PMF only.

B. A scale-invariant primordial magnetic field

Assuming statistical homogeneity and isotropy, the magnetic field correlation function in Fourier space is [29]

$$\langle b_i^*(\mathbf{k})b_j(\mathbf{k}') \rangle = \left[\left(\delta_{ij} - \frac{k_i k_j}{k^2} \right) S(k) + i \epsilon_{ijl} \frac{k_l}{k} A(k) \right] \times (2\pi)^3 \delta^3(\mathbf{k} - \mathbf{k}') \quad (8)$$

where repeated indices are summed over, $b_i(\mathbf{k})$ denotes the Fourier transform of the magnetic field at wave vector \mathbf{k} , $k = |\mathbf{k}|$, and $S(k)$ and $A(k)$ are the symmetric and antisymmetric (helical) parts of the magnetic field power spectrum.

The helical part of the power spectrum does not play a role in Faraday Rotation; only the symmetric part of the spectrum is relevant for us. On scales larger than the inertial scale, *i.e.* $k < k_I$, $S(k)$ will fall off as a power law. On scales smaller than a dissipative scale, *i.e.* $k > k_d$, the spectrum will get sharply cut-off. A second power-law behavior is possible for $k_I < k < k_d$. However, we shall assume that $k_I \approx k_d$, so that the magnetic field spectrum is given by a single power law behavior at all scales larger than the dissipation scale. These features can be summarized by [19]

$$S(k) = \begin{cases} \Omega_{B\gamma} \rho_\gamma \frac{32\pi^3 n}{k_I^3} \left(\frac{k}{k_I} \right)^{2n-3}, & 0 < k < k_{\text{diss}} \\ 0, & k_{\text{diss}} < k \end{cases} \quad (9)$$

where $\Omega_{B\gamma}$ is the ratio of cosmological magnetic and photon energy densities, and ρ_γ is the photon energy density.

For convenience, we define an “effective”, or “energy equivalent”, magnetic field strength

$$B_{\text{eff}} \equiv (8\pi \Omega_{B\gamma} \rho_\gamma)^{1/2} = 3.25 \times 10^{-6} \sqrt{\Omega_{B\gamma}} \text{ Gauss}. \quad (10)$$

A uniform magnetic field of strength B_{eff} will have the same energy density as a stochastic magnetic field with spectrum in Eq. (9).

Scale invariance for $k < k_d$ corresponds to $n = 0$, in which case the expressions in Eq. (9) are not well defined. One reason is that the energy density diverges logarithmically for a strictly scale invariant field. We get around this issue by only considering approximately scale invariant magnetic fields for which n is small. Note that, for scale invariant fields, B_{eff} is equal to the field strength smoothed over a scale λ (if it is larger than the dissipation scale), or B_λ , frequently used in the literature (*e.g.* in [3–5]).

As we have already noted, the galactic RM spectrum is approximately scale invariant. The RM induced by a scale invariant PMF is also scale invariant [11]. Hence the amplitudes of the galactic and PMF rotation measure spectra can be related directly for a scale invariant PMF.

For a scale-invariant angular spectrum C_ℓ , the quantity $\ell(\ell+1)C_\ell/2\pi$ is constant. Hence, one can define an amplitude

$$A_{\text{RM}} = \sqrt{\frac{L(L+1)C_L^{\text{RM}}}{2\pi}} \quad (11)$$

for the range of L over which the RM spectrum is approximately scale-invariant. One can see from Fig. 3 that this holds for the galactic RM for $L \lesssim 100$. Similarly, one can define an amplitude

$$A_\alpha = \sqrt{\frac{L(L+1)C_L^{\alpha\alpha}}{2\pi}} \quad (12)$$

The relation between the Faraday rotation angle in radians and the RM is given by $\alpha = c^2 \nu^{-2} \text{RM} = 10^{-4} \nu_{30}^{-2} \text{RM m}^2$ where $\nu_{30} \equiv \nu/30$ GHz. For example, a characteristic galactic RM of 30 rad/m² at 30 GHz gives a rotation angle of 3×10^{-3} rad, or 0.17°. The amplitudes of A_α in radians and A_{RM} in rad/m² are therefore also related via

$$A_\alpha = 10^{-4} \nu_{30}^{-2} A_{\text{RM}} \text{ m}^2. \quad (13)$$

To gain some intuition into the relative importance of the galactic RM prior to more detail forecasts in Sec III B, let us estimate the B_{eff} of scale-invariant PMF that gives RM comparable to that of our galaxy. For this, we can compare the amplitude A_α from PMF to the amplitude for galactic spectra at the same frequency. The relation between PMF and A_α involves integration along the line of sight (Eq. (1)). Rather than trying to find an approximate analytical solution, we use exact spectra found numerically in [11, 19]. From Fig. 1 of Ref. [11], one can infer that for a scale invariant PMF with $\Omega_{B\gamma} = 10^{-4}$, $(A_\alpha^{\text{PMF}})^2 \approx 2.43 \times 10^{-2} \text{ rad}^2$ at 30 GHz. We can then use Eqs. (13) and Eq. (10) to relate B_{eff} to A_{RM} :

$$B_{\text{eff}} \approx 0.021 A_{\text{RM}} \frac{\text{nG m}^2}{\text{rad}}. \quad (14)$$

From Fig. 3, we can see that $A_{\text{RM}} \approx 30 \text{ rad/m}^2$ for the galactic RM spectrum obtained without any sky cuts. It follows from Eq. (14) that this corresponds to a scale-invariant PMF with $B_{\text{eff}} \approx 0.6 \text{ nG}$. Such PMF are well below levels detectable by Planck through their FR signal, but can be detected at high significance by future sub-orbital and space-based experiments [11].

We can also estimate the peak value of the B-mode spectrum, $P_B \equiv \ell_{\text{peak}}(\ell_{\text{peak}}+1)C_{\ell_{\text{peak}}}^{BB}/2\pi$, in $(\mu\text{K})^2$, for a given A_{RM} and frequency. From Fig. 1, we see that $P_B \approx 0.03 (\mu\text{K})^2$ for a scale invariant PMF of 1 nG strength. Using this fact along with Eq. (14), we can deduce

$$P_B \approx \frac{0.03}{\nu_{30}^4} \left[\frac{B_{\text{eff}}}{\text{nG}} \right]^2 (\mu\text{K})^2 \approx \frac{10^{-5}}{\nu_{30}^4} \left[\frac{A_{\text{RM}} \text{ m}^2}{\text{rad}} \right]^2 (\mu\text{K})^2. \quad (15)$$

Thus, for a typical galactic A_{RM} of 30 rad/m², at 30 GHz, we should expect a peak in the B-mode spectrum of about $10^{-2} (\mu\text{K})^2$, which agrees with the blue dotted line in Fig. 1 corresponding to the unmasked galactic RM. In practice, the galactic plane is masked in all CMB experiments, *e.g.* the mask applied to Planck’s 30 GHz map only uses 0.6 of the sky. This significantly reduces the amplitude of the galactic RM spectrum and, as a consequence, the B-mode spectrum. This is shown as a blue

dashed line in Fig. 1. One can see that the galactic B-mode is at least one, and more likely two, orders of magnitude below the weak lensing signal, so there is almost no hope of seeing it even at a frequency as low as 30 GHz. Going a factor of ~ 3 higher in frequency, which is more typical in CMB studies, results in another factor of ~ 100 decrease in the B-mode spectrum.

One of the conclusions of this section is that the galactic RM is practically invisible in the BB auto-correlation. Hence, we should look at the mode-coupling estimators, as they are known to be much more sensitive to FR [11]. As shown in [11], future experiments can easily probe 0.1 nG strength PMF fields with the mode-coupling estimators.

C. The galactic rotation measure

A rotation measure (RM) map of Milky Way has been put together by Oppermann et al [16] based on an extensive catalog of Faraday rotation data of compact extragalactic polarized radio sources. The RM is strongest along the galactic plane, but remains significant at the poles. However, the latitude dependence of the rms RM disappears at latitudes higher than about 80° , where the dependence flattens out at a rms value of about 10 rad/m^2 . Oppermann et al [16] also presented the angular power spectrum of RM calculated after factoring out the latitude dependence. They find that $L(L+1)C_L^{\text{RM}} \propto L^{-0.17}$ at $L \lesssim 200$, which is very close to a scale-invariant spectrum.

Some insight into galactic RM on smaller scales is provided by Haverkorn et al [17]. They studied Stokes parameters, generated by diffuse polarized sources residing inside the galaxy, at several frequencies around 350 MHz. They focused on two separate patches away from the Galactic plane, each covering about 50 sq. deg. The rotation measures in both were less than 10 rad/m^2 . However, since they are looking at sources inside the galaxy, they only see a fraction of the total RM along each line of sight. Thus, their numbers cannot be directly compared to RM of [16]. Still their power spectrum gives a sense for the scale dependence of the total RM, and generally agrees with the flat nature of the large scale tail of the power spectrum of [16]. At a scale of about 0.3° ($L \sim 600$), they see evidence of a break in the spectrum, indicating a power law suppression of the RM power on small scales. Such a break in the spectrum is also present in the model of Minter and Spangler [18], whose analysis is based on a small set of RM data from extragalactic sources. They argued that on small scales the spectrum should be due to Kolmogorov turbulence. The corresponding scaling of $L(L+1)C_L^{\text{RM}}$ would be $L^{-2/3}$. To summarize, based on the evidence in [16–18], if we were to measure RM in a few degree patches near galactic poles, we would expect a RM spectrum that is roughly scale invariant at $L < 600$ turning into a $L^{-2/3}$ tail on smaller scales. As we will show in the next section, the quadratic estimator of the

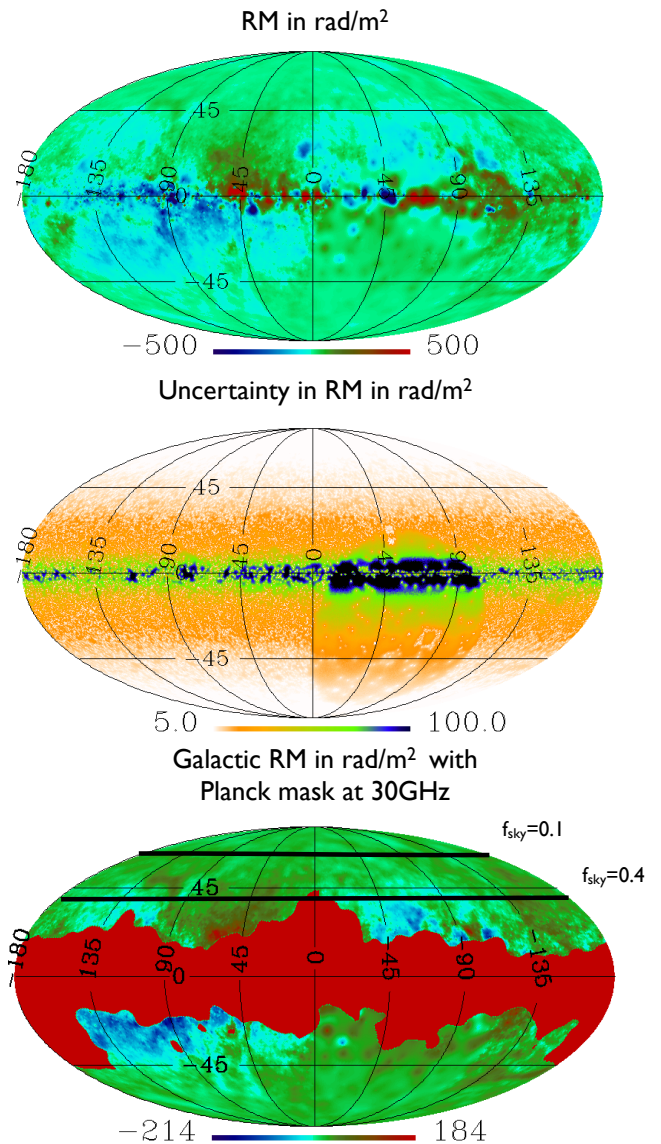


FIG. 2: Maps of RM from Oppermann et al [16]. The top panel shows the full sky map, the middle panel shows the associated error, while the bottom panel shows the map after applying the Planck 30 GHz sky cut. The bottom panel also shows lines of symmetric cuts corresponding to $f_{\text{sky}} = 0.4$ and $f_{\text{sky}} = 0.1$.

FR angle is largely uninformative for $L > 300$. Hence, we do not need a RM map with a resolution higher than that of Oppermann et al [16].

Note that the CMB polarization even in a small patch around the poles is affected by very long wavelength modes of variations of the RM. In terms of Eq. (3), lowest multipoles of α_{LM} contribute significantly to the much higher multipoles of B_{lm} . Thus, to predict the observability of the FR in CMB in a small patch one cannot simply use the high ℓ portion of the RM spectrum. We should use the full RM spectrum obtained from the RM after applying a mask normally used to block the galactic

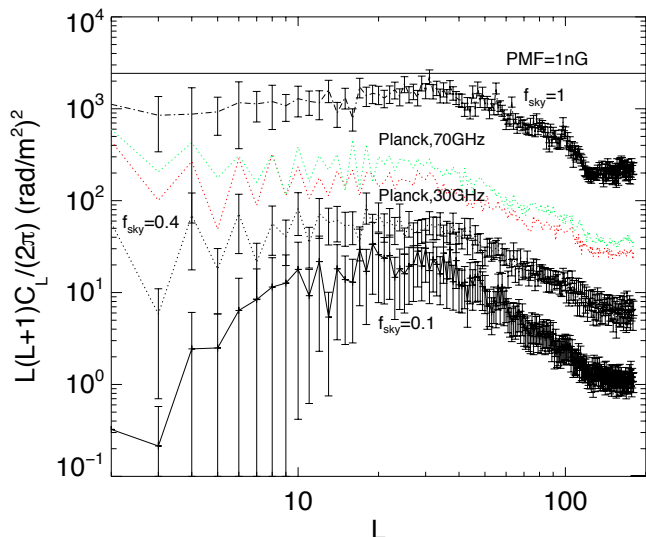


FIG. 3: The RM angular spectra, $L(L+1)C_L^{\text{RM}}/2\pi$, obtained from the RM map of Oppermann et al [16] with different cuts. Shown are the RM spectra corresponding to, from top to bottom, a scale-invariant PMF of 1 nG, galaxy with no sky cut, with a mask used by Planck for their 70 GHz map, a Planck mask for the 30 GHz map, and symmetric cuts corresponding to $f_{\text{sky}} = 0.4$ and $f_{\text{sky}} = 0.1$.

plane.

In Fig. 2 we show the RM map for our galaxy obtained from the Faraday rotation of extragalactic sources in units of rad/m^2 by Oppermann et al [16]. The top panel is the full map. The mid-panel shows the uncertainty in RM in rad/m^2 . Most of the signal and uncertainty come from the galactic disk. The bottom panel shows the RM map with part of the sky removed with a mask used for Planck’s mask 30 GHz map [30]. The bottom panel also shows lines of symmetric latitude cuts corresponding to sky fractions of $f_{\text{sky}} = 0.1$ and 0.4 .

In Fig. 3 we present the power spectra $L(L+1)C_L^{\text{RM}}/2\pi$ of the galactic RM under different symmetric sky cuts and two Planck mask cuts: one for 30 GHz with $f_{\text{sky}} = 0.6$, and one for 70 GHz with $f_{\text{sky}} = 0.7$. The figure also shows the RM spectrum from a scale-invariant PMF with $B_{\text{eff}} = 1$ nG. To calculate the galactic RM spectra, we first use HEALPix [31, 32] to find

$$\tilde{a}_{LM} = \int d\Omega W(\Omega) R(\Omega) Y_{LM}^*(\Omega), \quad (16)$$

where $R(\Omega)$ is the RM field, and $W(\Omega)$ is the mask which is 0 if a pixel is masked and 1 if it is not. We then evaluate

$$C_L^{\text{RM}} = \frac{1}{f_{\text{sky}}(2L+1)} \sum_{M=-L}^L \tilde{a}_{LM}^* \tilde{a}_{LM}, \quad (17)$$

which are the so-called “pseudo- C_L ” rescaled by f_{sky} .

The commonly used procedure for estimating C_L ’s from a partial sky is detailed in [33]. It assumes statistical isotropy and involves calculating a conversion matrix

that relates “pseudo- C_L ”, obtained from a partial sky, to the “full-sky” C_L . In Eq. (17), as a crude approximation, we ignore the mode-coupling and replace the matrix with a rescaling by the f_{sky} factor. Note that the galactic RM map is not isotropic and the “full-sky” spectrum reconstructed from a given patch is not the same as the actual spectrum evaluated from the full-sky. Thus, our estimates in Sec. III of the detectability of the galactic RM spectrum, and of the detectability of the PMF with the galactic RM as a foreground, are specific to particular masks. The error bars in Fig. 3 receive contributions from the uncertainty in the measurements of the RM map and from the cosmic variance.

III. DETECTABILITY PROSPECTS

We are interested in answering two questions: 1) *How well can CMB polarization experiments measure the galactic RM spectrum?* 2) *What bounds on a scale-invariant PMF can be placed from measurements of FR?* Both contributions, the galactic FR and the primordial FR, contribute in the same way to the quadratic estimators discussed in Sec. II A. Let $\hat{\alpha}_{LM}^{EB}$ be the estimator of the rotation angle that one reconstructs from linear combinations of quadratic terms $E_{lm}^* B_{l'm'}$. The variance in $\hat{\alpha}_{LM}^{EB}$, for a statistically isotropic rotation angle, is defined as

$$\langle \hat{\alpha}_{LM}^{EB*} \hat{\alpha}_{L'M'}^{EB} \rangle = \delta_{LL'} \delta_{MM'} \sigma_L^2, \quad (18)$$

with σ_L^2 given by [22, 24]

$$\sigma_L^2 = C_L^{\alpha\alpha} + N_L^{EB}, \quad (19)$$

where $C_L^{\alpha\alpha}$ is the rotation power spectrum, and N_L^{EB} is the part of the variance that does not depend on the rotation angle and contains contributions from variances of individual estimators $\hat{D}_{l'l'}^{LM, \text{map}}$ (see Eq. (6)), while accounting for their covariance. It is given by [22, 24]

$$(N_L^{EB})^{-1} = \frac{1}{\pi} \sum_{\ell\ell'} \frac{(2\ell+1)(2\ell'+1)[C_{\ell\ell'}^{EE} H_{\ell\ell'}^L]^2}{\tilde{C}_{\ell\ell'}^{EE} \tilde{C}_{\ell\ell'}^{BB}}, \quad (20)$$

where $\ell + \ell' + L = \text{even}$, and

$$\tilde{C}_{\ell}^{XX} \equiv [C^{XX}]_{\ell}^{\text{prim}} + f_{\text{DL}} [C^{XX}]_{\ell}^{\text{WL}} + I_{\ell}^{XX}, \quad (21)$$

is the measured spectrum, with XX standing for either EE or BB, that includes the primordial contribution, $[C^{XX}]^{\text{prim}}$, the weak lensing contribution, $[C^{XX}]^{\text{WL}}$, and the noise term associated with the experiment, I_{ℓ}^{XX} . We allow for the possibility of partial subtraction of the weak lensing contribution by introducing a de-lensing fraction, f_{DL} , in (21). The efficiency of de-lensing depends on the method used to de-lens [34, 35], as well as the noise and the resolution parameters of the experiment. In [35] it was found that the quadratic estimator method of de-lensing [27], which is similar but orthogonal [22, 23] to

the one we use to extract the FR rotation, can reduce the lensing contribution to BB by up to a factor of 7 as it reaches the white noise limit. On the other hand, the so-called iterative method [35] can further reduce the lensing contribution by a factor of 10 or larger. In our analysis we have only considered two cases – one with no de-lensing ($f_{\text{DL}} = 1$) and one with a factor of 100 reduction of the lensing B-mode ($f_{\text{DL}} = 0.01$). We adopt the latter optimistic assumption with the aim of illustrating the relative significance of lensing contamination for an experiment of given noise and resolution. Note that the numerator in Eq. (20) contains the unlensed E-mode spectrum, while the denominator includes the lensing contribution to E- and B-mode spectra. Predictions for both are readily obtained from CAMB [36, 37] for a given cosmological model.

The instrumental noise term, I_ℓ^{XX} , accounts for the detector noise as well as the suppression of the spectrum on scales smaller than the width of the beam [38]:

$$I_\ell^{EE} = I_\ell^{BB} = \Delta_P^2 \exp(\ell^2 \Theta_{\text{FWHM}}^2 / 8 \ln 2), \quad (22)$$

where Δ_P quantifies detector noise associated with measurements of CMB polarization and Θ_{FWHM} is the full width at half maximum of the Gaussian beam.

In the case of TB, the expression for the variance analogous to Eq. (20) is [24]

$$(N_L^{TB})^{-1} = \frac{1}{\pi} \sum_{\ell\ell'} \frac{(2\ell+1)(2\ell'+1)[C_{\ell'}^{TE} H_{\ell'}^L]^2}{\tilde{C}_{\ell'}^{TT} \tilde{C}_\ell^{BB}}. \quad (23)$$

Eq. (18) assumes that the distribution of the rotation angle is isotropic, and the angular brackets denote an ensemble average over many realizations of α as well as realizations of the primordial CMB sky. This is a well-motivated assumption for the PMF and for the galactic RM near galactic poles. Away from the poles, the galactic RM shows a strong dependence on the galactic latitude [16]. This means that the forecasted variance can differ from the actual uncertainty for larger values of f_{sky} , although we expect it to be of the correct order of magnitude. For the galactic RM map, we take the rotation angular spectrum to be $C_L^{\alpha\alpha} \equiv \nu^{-4} C_L^{RM}$, with C_L^{RM} calculated from the RM map of [16] after applying sky cuts, as plotted in Fig. 3 and explained in Sec. II C.

We will consider several sets of experimental parameters corresponding to ongoing, future and hypothetical experiments. Namely, we consider Planck's 30 GHz LFI and 100 GHz HFI channels based on actual performance characteristics [39], POLARBEAR [40] at 90 GHz with parameters compiled in [41], QUIET Phase II [42] at 40 GHz using the parameters compiled in [41], 30, 45, 70 and 100 GHz channels of a proposed CMBPol satellite [43], as well as an optimistic hypothetical sub-orbital and space-based experiments at 30 and 90 GHz. The assumed sky coverage (f_{sky}), resolution (Θ_{FWHM}), and instrumental noise (Δ_P) parameters are listed in Tables I and II.

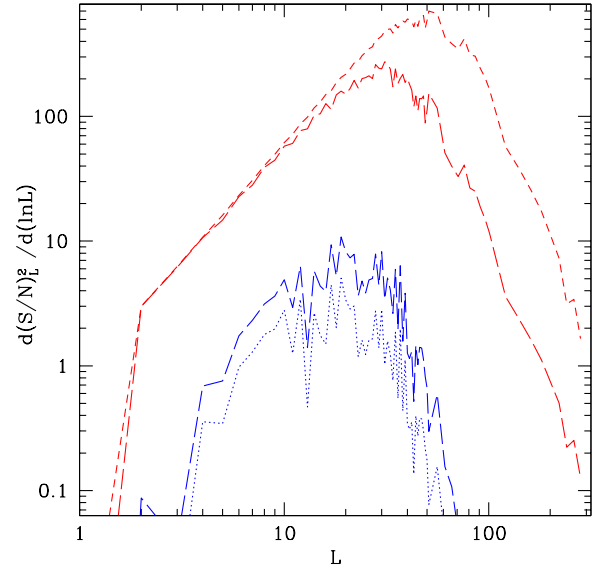


FIG. 4: Contribution of individual multipoles to the net SNR of detection of the galactic RM spectrum. Plotted are $d(S/N)_L^2/d\ln L$ for an optimistic 30 GHz sub-orbital experiment with (solid blue) and without (blue dot) de-lensing, as well as for a hypothetical future 30 GHz space probe with (red short dash) and without (red long dash) de-lensing ($f_{\text{DL}} = 0.01$). The spiky nature of the plot is due to the spikiness of the RM spectra, as seen in Fig. 3. Experimental parameters assumed in this plot are given in the text and in Table I.

A. Detectability of the galactic rotation measure

Let us estimate the significance level at which the galactic RM spectrum can be detected. The signal in this case is the rotation angle spectrum $C_L^{\alpha\alpha,G}$, related to the galactic RM spectrum via $C_L^{\alpha\alpha,G} = C_L^{\text{RM},G}/\nu^4$. Our forecasts will be specific to the spectra estimated after applying particular masks to the RM map from [16], and the RM spectra are different for different sky cuts, as can be seen in Fig. 3. The approximate expression for the variance is obtained under the assumption of statistically isotropic and Gaussian rotation angle:

$$\sigma_{C_L}^2 = \frac{2\sigma_L^2}{f_{\text{sky}}(2L+1)} \quad (24)$$

where σ_L^2 is the variance of the estimator $\hat{\alpha}_{LM}^{XB}$ defined in Eq. (19), and X stands for either E or T, depending on whether one uses the EB or TB estimator. The total SNR squared of the detection of the galactic FR spectrum is the sum of $(C_L^{\alpha\alpha,G}/\sigma_{C_L})^2$ at each L :

$$\left(\frac{S}{N}\right)_{XB}^2 = \sum_{L=1}^{L_{\text{max}}} \frac{f_{\text{sky}}(2L+1)[C_L^{\alpha\alpha,G}]^2}{2[C_L^{\alpha\alpha,G} + N_L^{XB}]^2}. \quad (25)$$

Note that even for a small sky coverage, the SNR receives a non-zero contribution from the smallest multipoles L

Name - freq (GHz)	f_{sky}	FWHM (arcmin)	$\Delta_P(\mu\text{K-arcmin})$	$(S/N)_{EB}$ (+DL)	$(S/N)_{TB}$ (+DL)	$(S/N)_{BB}$ (+DL)
Planck LFI - 30	0.6	33	240	5.3E-4 (same)	2.2E-3 (same)	2.3E-4 (same)
Planck HFI - 100	0.7	9.7	106	1.4E-3 (same)	7.5E-4 (same)	6E-5 (same)
Polarbear - 90	0.024 ^a	6.7	7.6	1.3E-2 (1.5E-2)	1.6E-3 (2.0E-3)	4.6E-4 (6.0E-4)
QUIET II - 40	0.04 ^a	23	1.7	0.3 (0.8)	0.05 (0.2)	0.02 (0.08)
CMBPOL - 30	0.6	26	19	1.0 (same)	0.4 (same)	0.05 (same)
CMBPOL - 45	0.7	17	8.25	2.1 (2.3)	0.8 (0.9)	0.12 (0.15)
CMBPOL - 70	0.7	11	4.23	2.0 (2.6)	0.6 (0.9)	0.08 (0.14)
CMBPOL - 100	0.7	8	3.22	1.4 (2.0)	0.3 (0.6)	0.03 (0.07)
Suborbital - 30	0.1	1.3	3	2.0 (3.1)	0.3 (0.7)	0.08 (0.2)
Space - 30	0.6	4	1.4	18 (28)	7 (14)	5 (30)
Space - 90	0.7	4	1.4	3.3 (6.8)	1.0 (2.4)	0.09 (0.64)

TABLE I: S/N of the overall detection of the galactic RM spectrum with Planck, Polarbear, QUIET, CMBPOL and optimistic future sub-orbital and space experiments. Results are presented without and with (+DL) de-lensing by a factor $f_{\text{DL}} = 0.01$. (^a based on 0.1 of RM sky.)

of the rotation angle. This is because large angle features of RM couple small angle features of CMB, and there will be $l'l'$ pairs (see Eq. (7)) giving an estimate of RM at small L no matter how small f_{sky} is. However, the smaller the sky coverage, the smaller is the number of available $l'l'$ pairs leading to larger statistical errors.

In addition to the EB estimator, one may also want to know how detectable the Milky Way RM is in the B-mode spectrum. In this case, the signal is the B-mode spectrum generated by the FR inside the galaxy, $C_L^{BB,G}$ (see Fig. 1). The squared SNR is

$$\left(\frac{S}{N}\right)_{BB}^2 = \sum_{L=2}^{L_{max}} \frac{f_{\text{sky}}}{2} (2L+1) \left(\frac{C_L^{BB,G}}{\tilde{C}_L^{BB}}\right)^2. \quad (26)$$

where \tilde{C}_L^{BB} is given by Eq. (21) and includes contributions from galaxy, weak lensing and instrumental noise.

In Fig. 4, we plot contributions to the net SNR in detection of the galactic RM spectrum, given by Eq. (4), received per $\ln L$. We show four different cases, all at 30 GHz, corresponding to hypothetical future sub-orbital and space based experiments, with and without de-lensing by a factor $f_{\text{DL}} = 0.01$. We assume that the sub-orbital experiment will cover $f_{\text{sky}} = 0.1$ with $\Delta_P = 3\mu\text{K-arcmin}$ and FWHM of $1.3'$, while the space-based probe will cover $f_{\text{sky}} = 0.6$ (based on Planck's 30 GHz sky mask) with $\Delta_P = 1.4\mu\text{K-arcmin}$ and FWHM of $4'$. Note that, as shown in Fig. 3, elimination of the galactic plane significantly reduces the amplitude of the galactic RM spectrum signal. Thus, the overall SNR of detection of the galactic RM spectrum is only of $\mathcal{O}(1)$ for the most optimistic sub-orbital experiment, with de-lensing making a relatively minor difference. In contrast, a space-based probe can detect the galactic RM at a high confidence level, with most of the signal coming from $4 < L < 100$. This means that CMB polarization can, in principle, be used to reconstruct the galactic RM map at a resolution of up to a degree. De-lensing the CMB maps can further improve the accuracy of the reconstruction.

In Table I, we forecast the SNR in detection of the galactic RM spectrum for several ongoing, proposed and hypothetical experiments. For experiments with $f_{\text{sky}} < 0.1$, such as QUIET and POLARBEAR, we use C_L^{RM} with the $f_{\text{sky}} = 0.1$ cut of the RM map (the bottom line in Fig. 3) around the galactic plane. Thus, our estimates assume that QUIET and POLARBEAR will observe in patches that are close to the galactic poles where statistical properties of the galactic RM become independent of the exact size of the patch. This expectation is justified by the fact that latitude dependence essentially disappears as one approaches the poles, which is quantified in Fig. 1 of [16].

We separately show results based on the EB, TB and BB estimators, with and without de-lensing. The results allow us to make the following conclusions. Firstly, the galactic RM will be invisible in Planck's polarization maps. Secondly, the galactic RM spectrum is unlikely to be detected by a sub-orbital experiment covering a small fraction of the sky near the galactic poles, at least not via the mode-coupling quadratic estimators or its contribution to the B-mode spectrum, unless very optimistic assumptions are made about its resolution and sensitivity. Thirdly, space-based polarization probes, such as the proposed CMBPOL mission, should take the galactic RM into account. We note that our analysis does not cover the possibility of the galactic RM being detected directly from Eq. (2) by utilizing the frequency dependence of Stokes parameters. This may turn out to be a more sensitive method for future multi-frequency CMB experiments with sufficiently low instrumental noise. We leave investigation of this possibility for future work.

Name - freq (GHz)	$f_{\text{sky}} (f_{\text{sky}}^{\text{opt}})$	FWHM (arcmin)	$\Delta_P (\mu\text{K}\cdot\text{arcmin})$	$B_{\text{eff}} (2\sigma, \text{nG})$	+DL (nG)	+DL+DG (nG)
Planck LFI - 30	0.6	33	240	16 ^b	same	same
Planck HFI - 100	0.7	9.7	106	23	same	same
Polarbear - 90	0.024 ^a	6.7	7.6	3.3	3.0	same
QUIET II - 40	0.04 ^a	23	1.7	0.46	0.26	0.25
CMBPOL - 30	0.6	26	19	0.56	0.55	0.51
CMBPOL - 45	0.7	17	8.25	0.38	0.35	0.29
CMBPOL - 70	0.7	11	4.23	0.39	0.32	0.26
CMBPOL - 100	0.7	8	3.22	0.52	0.4	0.34
Suborbital - 30	0.1	1.3	3	0.09	0.07	0.05
Suborbital - 90	0.1	1.3	3	0.63	0.45	same
Space - 30	0.6 (0.2)	4	1.4	0.06	0.04	0.02
Space - 90	0.7 (0.4)	4	1.4	0.26	0.15	0.12

TABLE II: The expected 2σ bound in nano-Gauss on the strength of a scale-invariant PMF. Without de-lensing and with de-lensing (+DL) by a factor $f_{\text{DL}} = 0.01$, and with additional removal of the galactic RM by a factor $f_{\text{DG}} = 0.1$ (+DL+DG). Note that for full sky experiments, there is an optimal sky cut ($f_{\text{sky}}^{\text{opt}}$) that gives the best bounds on the PMF. (^a based on 0.1 of RM sky; ^b from TB estimator.)

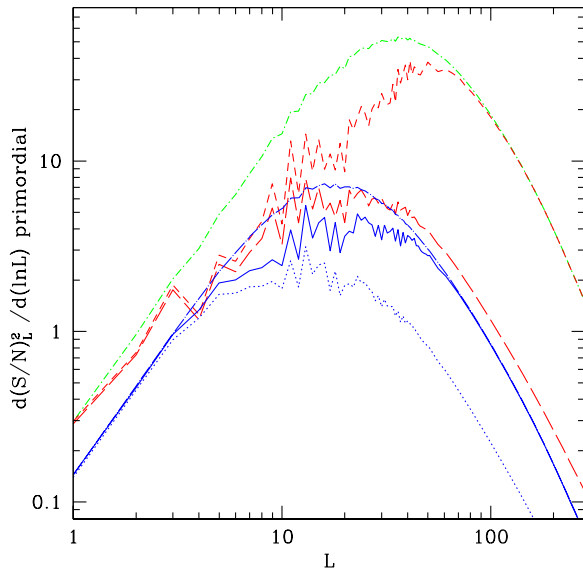


FIG. 5: Contribution of individual multipoles to the net SNR of detection of the PMF of 0.1 nG. Plotted are $d(S/N)_L^2/d\ln L$ for an optimistic 30 GHz sub-orbital experiment without de-lensing (blue dot), after de-lensing ($f_{\text{DL}} = 0.01$, solid blue) and after de-lensing and partially subtracting the galactic RM ($f_{\text{DG}} = 0.1$, blue long dash-dot), as well as for a hypothetical future 30 GHz space probe with (red short dash) and without (red long dash) de-lensing ($f_{\text{DL}} = 0.01$), as well as with partial ($f_{\text{DG}} = 0.1$) subtraction of the galactic RM (green dash-dot). The red short and long dash lines correspond to $f_{\text{sky}}^{\text{opt}} = 0.2$, while the green dash-dot uses $f_{\text{sky}}^{\text{opt}} = f_{\text{sky}} = 0.5$. The lines are spiky because the RM spectra, as seen in Fig. 3, contribute to then the noise part of the SNR. Note that spikes disappear when the galactic RM is partially subtracted. Experimental parameters assumed in this plot are given the text and in Table II.

B. Detectability of the primordial magnetic field

The SNR of the detection of the primordial FR rotation angle is given by

$$\left(\frac{S}{N}\right)_{XB}^2 = \sum_{L=1}^{L_{\text{max}}} \frac{f_{\text{sky}}(2L+1)[C_L^{\alpha\alpha,PMF}]^2}{2[C_L^{\alpha\alpha,PMF} + f_{\text{DG}}C_L^{\alpha\alpha,G} + N_L^{XB}]^2} \quad (27)$$

where X stands for either E or T, depending on whether one uses the EB or TB estimator, $C_L^{\alpha\alpha,PMF}$ is the primordial contribution, while f_{DG} is the “de-galaxing” factor, *i.e.* the fraction of the galactic rotation angle spectrum that is known from other sources and can be subtracted.

As in the case of the galactic RM, the SNR receives a non-zero contribution from all multipoles L , including the smallest, even for a small sky coverage. In the case when a large fraction of the sky is available, there is an optimal cut of the sky, $f_{\text{sky}}^{\text{opt}}$, for which the S/N is maximal. This is because the galactic RM contribution is weaker when large parts of the sky are cut, but there are more available modes when more of the sky is kept. In what follows, we will state when values of $f_{\text{sky}}^{\text{opt}}$ are different from f_{sky} .

In Fig. 5, we plot contributions per $\ln L$ to the net SNR in detection of the FR from a scale-invariant PMF with $B_{\text{eff}} = 0.1$ nG for the same two hypothetical experiments considered in Fig. 4. In addition to the four cases considered in Fig. 4, the green dot-dash line shows the case when the galactic contribution is partially subtracted for the space-based probe with $f_{\text{DG}} = 0.1$. A few observations can be made from this plot. First is that both experiments can detect a 0.1 nG PMF at high significance, which constitutes a big improvement on prospects of detecting a PMF in CMB via non-FR signatures [3–5]. Second is that de-lensing makes a significant difference for both the space-based and sub-orbital experiments. Third is that subtracting the galactic RM moderately improves

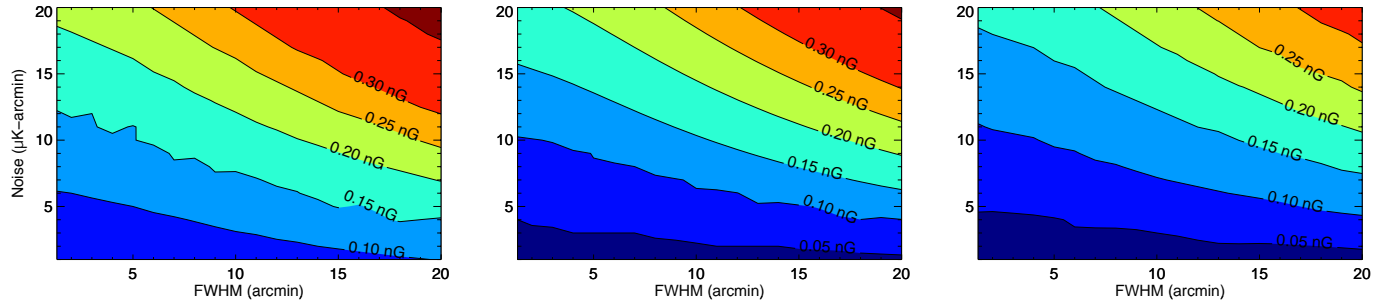


FIG. 6: Contour plots of the 2σ bound on B_{eff} (in nG) in the instrumental noise – CMB resolution plane, with the frequency channel taken to be 30 GHz. The left panel shows the case with no de-lensing ($f_{\text{DL}} = 1$) and without subtracting the Milky Way RM ($f_{\text{DG}} = 1$). The middle panel is with $f_{\text{DL}} = 0.01$, while the right panel is with $f_{\text{DL}} = 0.01$ and $f_{\text{DG}} = 0.1$. It is assumed that up to 0.6 of the sky is available and an optimal sky cut is found in each case.

the detection at multipoles in the $4 \lesssim L \lesssim 70$ range. Finally, we can see that most of the information comes from $4 < L < 200$, meaning that future CMB experiments can reconstruct FR maps corresponding to PMF of 0.1 nG strength up to a degree resolution.

In Table II we present our forecasts for 2σ bounds on B_{eff} that can be expected from various ongoing and future CMB experiments. We present results obtained from the EB estimator, because they lead to the strongest bounds, except for the case of Planck’s 30 GHz channel, for which the TB estimator gives better constraints. For each experiment, we check the effect of de-lensing (+DL) with $f_{\text{DL}} = 0.01$ as well as further partial subtraction of the galactic RM (+DL+DG) with $f_{\text{DG}} = 0.1$. The optimal sky cuts are indicated when relevant. One of the interesting facts one can extract from this table is that very competitive bounds can be placed by POLARBEAR and QUIET, while even $\mathcal{O}(10^{-11}\text{G})$ fields can be constrained in principle by future experiments.

To show the dependence of the PMF bound on the instrumental noise and resolution, we plot contours of constant 2σ bounds on B_{eff} in Fig. 6. The three panels show the cases with and without de-lensing and with an additional partial subtraction of the galactic RM. An optimal sky cut was used for each set of parameters.

IV. SUMMARY AND OUTLOOK

We have studied the detectability of a scale-invariant PMF due to FR of the CMB using polarization correlators in the presence of the foreground imposed by the Milky Way magnetic field. We have found that the galactic RM is not a serious barrier to observe a scale-invariant PMF and that the EB quadratic correlator is in general more powerful than the BB correlator.

We have also studied the detectability of the PMF as a function of the sky coverage. We find that suborbital experiments can be almost as effective as space borne exper-

iments, and the obstruction caused by the galaxy is relatively weak if the observed patch is near the poles. Also, as the mode-coupling correlations of CMB are mostly sourced by the largest scale features (low L) of the rotation measure, a full sky CMB map is not necessary to access the PMF on the largest scales.

Our results on the sensitivities of various experiments to the galactic magnetic field are summarized in Table I. Similarly in Table II we show the effective magnetic field strength that can be constrained by those experiments, taking into account the lensing of the CMB and the FR due to the Milky Way. The dependence of the observable PMF to the parameters of the experiment are shown in Fig. 6.

Here we have focussed on the observability of CMB FR at a single frequency. Cross-correlating polarization maps at multiple frequencies with comparable sensitivity to FR can further boost the significance of detection. We will address this possibility in a future publication. Also, frequency dependence of polarization can be used to separate out FR induced B-modes from those induced by gravitational waves.

Acknowledgments

We thank the two anonymous referees for their careful reading of the initially submitted version and constructive suggestions that helped to improve the paper. We are grateful to Niels Oppermann and collaborators [16] for making their rotation measure maps publicly available at [44]. Some of the results in this paper have been derived using the HEALPix [31, 32] package. LP and TV benefited from previous collaborations with Amit Yadav. We thank Steven Gratton, Yin-Zhe Ma, Phil Mauskopf and Vlad Stolyarov for discussions and helpful comments. SD is supported by a SESE Exploration postdoctoral fellowship; LP is supported by an NSERC Discovery grant; TV is supported by the DOE at Arizona State University.

- [1] D. Grasso and H. R. Rubinstein, Phys. Rept. **348**, 163 (2001) [[astro-ph/0009061](#)].
- [2] L. M. Widrow, Rev. Mod. Phys. **74**, 775 (2002) [[astro-ph/0207240](#)].
- [3] P. A. R. Ade *et al.* [Planck Collaboration], [arXiv:1303.5076](#) [astro-ph.CO].
- [4] D. Paoletti, F. Finelli and F. Paci, Mon. Not. Roy. Astron. Soc. **396** (2009) 523 [[arXiv:0811.0230](#) [astro-ph]].
- [5] D. Paoletti and F. Finelli, [arXiv:1208.2625](#) [astro-ph.CO].
- [6] M. S. Turner and L. M. Widrow, Phys. Rev. D **37**, 2743 (1988).
- [7] B. Ratra, Astrophys. J. **391**, L1 (1992).
- [8] T. Kahniashvili, Y. Maravin, A. Natarajan, N. Battaglia and A. G. Tevzadze, Astrophys. J. **770**, 47 (2013) [[arXiv:1211.2769](#) [astro-ph.CO]].
- [9] R. A. C. Croft, D. H. Weinberg, M. Bolte, S. Burles, L. Hernquist, N. Katz, D. Kirkman and D. Tytler, Astrophys. J. **581**, 20 (2002) [[astro-ph/0012324](#)].
- [10] T. Kahniashvili, Y. Maravin and A. Kosowsky, Phys. Rev. D **80**, 023009 (2009) [[arXiv:0806.1876](#) [astro-ph]].
- [11] A. Yadav, L. Pogosian and T. Vachaspati, Phys. Rev. D **86**, 123009 (2012) [[arXiv:1207.3356](#) [astro-ph.CO]].
- [12] T. Vachaspati, Phys. Lett. B **265**, 258 (1991).
- [13] R. Durrer and C. Caprini, JCAP **0311**, 010 (2003) [[astro-ph/0305059](#)].
- [14] K. Jedamzik and G. Sigl, Phys. Rev. D **83**, 103005 (2011) [[arXiv:1012.4794](#) [astro-ph.CO]].
- [15] K. Jedamzik and T. Abel, [arXiv:1108.2517](#) [astro-ph.CO].
- [16] N. Oppermann, H. Junklewitz, G. Robbers, M. R. Bell, T. A. Ensslin, A. Bonafede, R. Braun and J. C. Brown *et al.*, [arXiv:1111.6186](#) [astro-ph.GA].
- [17] M. Haverkorn, P. Katgert and A. G. de Bruyn, Astron. Astrophys. **403**, 1045 (2003) [[astro-ph/0303644](#)].
- [18] A. H. Minter and S. R. Spangler, Ap. J. **458**, 194 (1996).
- [19] L. Pogosian, A. P. S. Yadav, Y. -F. Ng and T. Vachaspati, Phys. Rev. D **84**, 043530 (2011) [Erratum-ibid. D **84**, 089903 (2011)] [[arXiv:1106.1438](#) [astro-ph.CO]].
- [20] A. Kosowsky and A. Loeb, Astrophys. J. **469**, 1 (1996) [[astro-ph/9601055](#)].
- [21] D. D. Harari, J. D. Hayward and M. Zaldarriaga, Phys. Rev. D **55**, 1841 (1997) [[astro-ph/9608098](#)].
- [22] M. Kamionkowski, Phys. Rev. Lett. **102**, 111302 (2009) [[arXiv:0810.1286](#) [astro-ph]].
- [23] A. P. S. Yadav, R. Biswas, I. M. Su and M. Zaldarriaga, Phys. Rev. D **79**, 123009 (2009) [[arXiv:0902.4466](#) [astro-ph.CO]].
- [24] V. Gluscevic, M. Kamionkowski and A. Cooray, Phys. Rev. D **80**, 023510 (2009) [[arXiv:0905.1687](#) [astro-ph.CO]].
- [25] V. Gluscevic, D. Hanson, M. Kamionkowski and C. M. Hirata, [arXiv:1206.5546](#) [astro-ph.CO].
- [26] A. P. S. Yadav, M. Shimon and B. G. Keating, Phys. Rev. D **86**, 083002 (2012) [[arXiv:1207.6640](#) [astro-ph.CO]].
- [27] W. Hu and T. Okamoto, Astrophys. J. **574**, 566 (2002) [[astro-ph/0111606](#)].
- [28] A. R. Pullen and M. Kamionkowski, Phys. Rev. D **76**, 103529 (2007) [[arXiv:0709.1144](#) [astro-ph]].
- [29] Monin A. S., Iaglom A. M., Statistical fluid mechanics: Mechanics of turbulence. Volume 2, Cambridge, Mass., MIT Press, (1975).
- [30] <http://pla.esac.esa.int/pla/aio/planckProducts.html>
- [31] <http://healpix.jpl.nasa.gov>
- [32] K. M. Gorski, E. Hivon, A. J. Banday, B. D. Wandelt, F. K. Hansen, M. Reinecke and M. Bartelman, Astrophys. J. **622**, 759 (2005) [[astro-ph/0409513](#)].
- [33] E. Hivon, K. M. Gorski, C. B. Netterfield, B. P. Crill, S. Prunet and F. Hansen, Astrophys. J. **567**, 2 (2002) [[astro-ph/0105302](#)].
- [34] C. M. Hirata and U. Seljak, Phys. Rev. D **67**, 043001 (2003) [[astro-ph/0209489](#)].
- [35] U. Seljak and C. M. Hirata, Phys. Rev. D **69**, 043005 (2004) [[astro-ph/0310163](#)].
- [36] <http://camb.info/>
- [37] A. Lewis, A. Challinor and A. Lasenby, Astrophys. J. **538**, 473 (2000) [[arXiv:astro-ph/9911177](#)].
- [38] J. R. Bond, G. Efstathiou and M. Tegmark, Mon. Not. Roy. Astron. Soc. **291**, L33 (1997) [[astro-ph/9702100](#)].
- [39] P. A. R. Ade *et al.* [Planck Collaboration], [arXiv:1303.5062](#) [astro-ph.CO].
- [40] B. Keating, S. Moyerman, D. Boettger, J. Edwards, G. Fuller, F. Matsuda, N. Miller and H. Paar *et al.*, [arXiv:1110.2101](#) [astro-ph.CO].
- [41] Y. -Z. Ma, W. Zhao and M. L. Brown, JCAP **1010**, 007 (2010) [[arXiv:1007.2396](#) [astro-ph.CO]].
- [42] D. Samtleben [QUIET Collaboration], Nuovo Cim. B **122**, 1353 (2007) [[arXiv:0802.2657](#) [astro-ph]].
- [43] D. Baumann *et al.* [CMBPol Study Team Collaboration], AIP Conf. Proc. **1141**, 10 (2009) [[arXiv:0811.3919](#) [astro-ph]].
- [44] <http://www.mpa-garching.mpg.de/ift/faraday/>